JOURNAL OF SYNCHROTRON RADIATION

ISSN 1600-5775

Effect of the third undulator field harmonic on spontaneous and stimulated undulator radiation

K. V. Zhukovsky*

Department of Theoretical Physics, Faculty of Physics, M. V. Lomonosov Moscow State University, Moscow 119991, Russian Federation. *Correspondence e-mail: zhukovsk@physics.msu.ru

Received 3 January 2019
Accepted 13 June 2019

Edited by M. Yamamoto, RIKEN SPring-8 Center, Japan

Keywords: undulator radiation; harmonics; free-electron laser.

The effect of undulator field harmonics on spontaneous and stimulated undulator radiation, both on and off the undulator axis, is studied. Bessel factors for the undulators with field harmonics have been analytically calculated and numerically verified. The influence of the third undulator field harmonic on single-pass free-electron laser radiation is explored. Harmonic generation at the LCLS and SPring-8 free-electron lasers is modeled and analyzed.

1. Introduction

In an undulator, electrons with high relativistic factor γ pass through a spatially periodic magnetic field and emit undulator radiation (UR). Undulators in free-electron lasers (FELs) generate coherent UR (McNeil & Thompson, 2010; Pellegrini *et al.*, 2016; Huang & Kim, 2007; Saldin *et al.*, 2000; Margaritondo & Ribic, 2011; Pellegrini, 2016). This process can be modeled numerically or using phenomenological formulae. The former approach implies a numerical solution of an equation system for the electron motion and interaction with the wavefield. This can be done in one or three dimensions and requires serious computational resources and trained personnel. The analytical approach gives an effective FEL description and can reproduce fairly well the harmonic growth in real devices. Going beyond the usual assumption of a sinusoidal undulator on-axis field, we study the following undulator field,

$$\mathbf{H} = \big(0, H_0\{0 + [\sin(zk_\lambda) + d\sin(hzk_\lambda)]\}, 0\big), \qquad (1)$$

with amplitude H_0, main period λ_u, $k_\lambda = 2\pi/\lambda_u$, second period λ_u/h and second amplitude dH_0, $h = 2, 3, 4\ldots$. A relatively weak, $h \simeq 0.1$–0.5, third field harmonic can be present in real devices. There have been controversial conclusions (Zhukovsky, 2015*a*,*b*, 2016*a*,*b*; Jeevakhan & Mishra, 2011; Mishra *et al.*, 2009; Jia, 2011) on its effect on the UR harmonics. We rigorously obtained the analytical expressions for the Bessel functions T_n for the undulator field (1) by computing the radiation integral

$$\frac{\mathrm{d}^2 I}{\mathrm{d}\omega\,\mathrm{d}\Omega} = \frac{e^2}{4\pi^2 c}\left|\omega\int_{-\infty}^{\infty}\big[\mathbf{n}\times(\mathbf{n}\times\boldsymbol{\beta})\big]\exp[i\omega(t-\mathbf{nr}/c)]\,\mathrm{d}t\right|^2, \qquad (2)$$

where

$$\mathbf{n} \cong \big\{\theta\cos\phi, \theta\sin\phi, 1-\theta^2/2\big\}$$

where $\mathbf{r}$ are coordinates and $\boldsymbol{\beta}$ are velocities.

The exponential in (2) yields the generalized Bessel function

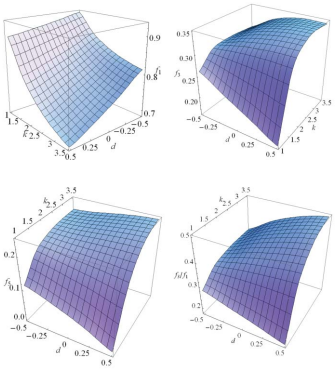

$$J_n = \frac{1}{2\pi}\int_0^{2\pi} \cos\Big\{\xi_1 \sin\phi + \xi\sin(2\phi) + \xi_- \sin[(h-1)\phi] + \xi_+ \sin[(h+1)\phi] + \xi_h \sin(2h\phi) + n\phi\Big\}\,\mathrm{d}\phi, \quad (3)$$

which involves the parameter $k = H_0\lambda_u e/2\pi mc^2$ as follows,

$$\xi = \frac{nk^2/4}{1+(k^2/2)[1+(d^2/h^2)]},$$
$$\xi_1 = \frac{8\xi\gamma\theta}{k}, \qquad \xi_- = \frac{4d\xi}{h(h-1)}, \quad (4)$$
$$\xi_+ = \frac{4d\xi}{h(h+1)}, \qquad \xi_h = \frac{d^2\xi}{h^3}.$$

The Bessel coefficients $f_{n;x} = |T_{n;x}|$ for the harmonic $n = 1, 2, 3, \ldots$ taking account of the off-axis radiation at angle θ read as follows,

$$T_{n,x} = J_{n-1} + J_{n+1} + \frac{d}{h}\big(J_{n+h} + J_{n-h}\big) + aJ_n, \quad T_{n,y} = bJ_n, \quad (5)$$

where $a = 2\gamma\theta\cos\phi/k$, $b = 2\gamma\theta\sin\phi/k$, θ is the off-axis angle and ϕ is the polar angle. The wavelength of the nth UR harmonic from a planar undulator is

$$\lambda_n = \frac{\lambda_u}{2n\gamma^2}\big[1 + k_{\rm eff}^2 + (\gamma\theta)^2\big], \quad k_{\rm eff}^2 = \frac{k^2}{2}\left(1 + \frac{d^2}{h^2}\right). \quad (6)$$

In the following we present the Bessel functions also for the elliptic undulator with field harmonics. We explore in particular the effect of the third undulator field harmonic on the UR. We compute analytically the UR intensity in the field (1) and compare it with proper numerical results. Furthermore, we calculate the UR intensity for an elliptic undulator and we model the harmonic power in several FEL experiments. We analyze the harmonic generation in the SPring-8 and LCLS FELs for several setups and study possible effects of the undulator field harmonics.

2. Spontaneous UR and validation of the Bessel factors

The intensity of the spontaneous UR in the undulator with N periods taking into account the energy spread σ_e is given by the convolution

$$\frac{\mathrm{d}^2 I_n}{\mathrm{d}\omega\,\mathrm{d}\Omega} \cong C\Big(\big|T_{n,x}\big|^2 + \big|T_{n,y}\big|^2\Big)\int_{-\infty}^{\infty} \exp\big(-\varepsilon^2/2\sigma_e^2\big) \times \mathrm{sinc}^2(\nu_n + 2\pi nN\varepsilon)\,\mathrm{d}\varepsilon, \quad (7)$$

where $C = e^2N^2\gamma^2k^2n^2/c\sqrt{2\pi}\sigma_e(1+k_{\rm eff}^2)^2$, e is the electron charge, c is the speed of light and $\nu_n = 2\pi nN[(\lambda_n/\lambda) - 1]$ is the detuning parameter. On the axis of a common planar undulator, where $d = \theta = 0$, only x-polarization is radiated. The proper Bessel coefficient $f_{n,x} = J_{(n-1)/2}(-\xi_0) + J_{(n+1)/2}(-\xi_0)$ contains common Bessel functions $J_n(\xi_0 \equiv \xi|_{d=0})$. In the presence of the additional field harmonic the Bessel coefficients f_n of the planar undulator (1) depend on k and d [see (3)–(5)]. An example of such a dependence for $h = 3$ is shown in Fig. 1. The energy spread decreases the effective value of f_n as shown in Fig. 2.

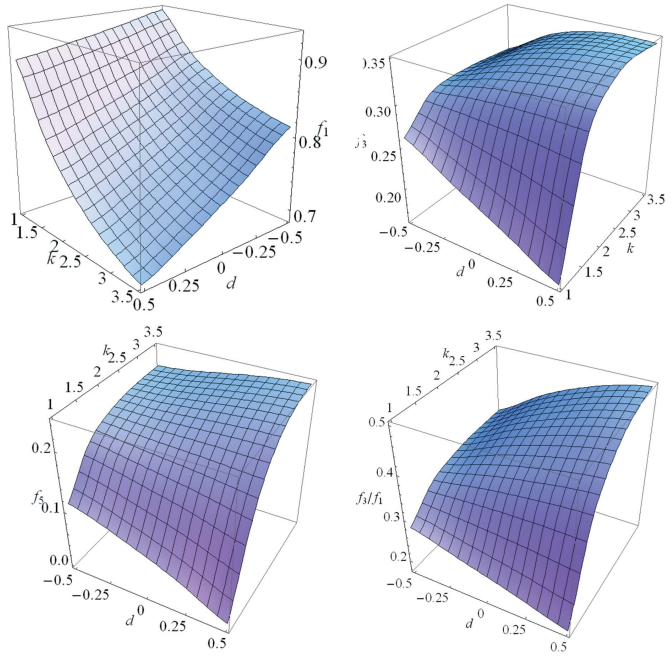

Figure 1
Bessel coefficients $f_{1,3,5}$ and their ratio f_3/f_1 for k and d, $h = 3$.

It follows from the analysis of Fig. 1 that the Bessel factors and the UR harmonics weakly sense the third undulator field harmonic for $k \cong 1.5$. For $k < 1.5$ the third field harmonic with negative phase, $d < 0$, slightly enhances the UR harmonics. The positive phase of the field harmonic, $d > 0$, weakens the UR harmonics (see Fig. 1). For $k > 1.5$ the effect of the field dH_0 in (1) is the opposite: high UR harmonics with $n = 3, 5, \ldots$ become stronger for $d > 0$ and weaker for $d < 0$ (see Fig. 1). This observation clarifies contradicting reports on the harmonic behavior in various references (Zhukovsky, 2015*a*,*b*, 2016*a*,*b*; Jeevakhan & Mishra, 2011; Mishra *et al.*, 2009; Jia,

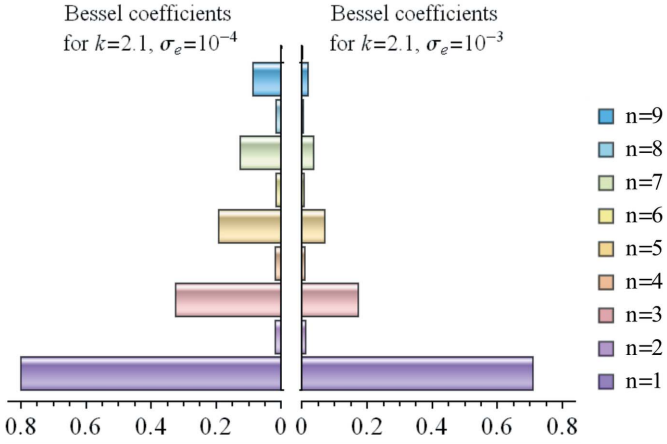

Figure 2
Bessel factors, weighted with the energy spread $\sigma_e = 10^{-4}$ (left) and $\sigma_e = 10^{-3}$ (right), $\gamma\theta = 0.0123$, $k = 2.1$, $h = d = 0$.

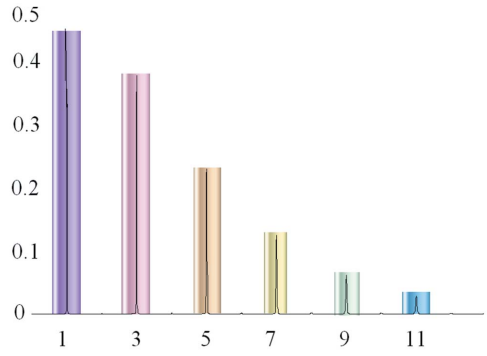

Figure 3
Spontaneous UR harmonic intensity (in relative units) from the undulator with $k = 2.1$, $h = 3$, $d = +0.42$, $\sigma_e = 1.5 \times 10^{-3}$ for the harmonic number n.

2011). Indeed (see Fig. 1), for $k > 1.5$ the rate $f_{3,5}/f_1$ increases for higher values of $d > 0$ and decreases for lower values $d < 0$. For $k < 1.5$, on the contrary, the rate $f_{3,5}/f_1$ of high harmonics increases for lower values of $d < 0$. The variation of $f_{3,5}/f_1$ can be about $\pm 20\%$, depending on d.

We have computed the UR harmonic intensity numerically using the *SPECTRA* program (Tanaka & Kitamura, 2001; Tanaka, 2014), which allows field harmonics for planar undulators. Examples for $k = 2.1$, $h = 3$, $d = \pm 0.42$, $\sigma_e = 1.5 \times 10^{-3}$ are shown in Figs. 3 and 4, where color bars show our analytical results and thin black lines show the data from *SPECTRA*. The agreement is quite good. The ratio I_n/I_1 of the spontaneous UR harmonic intensities changes, for $d = \pm 0.42$, by about $\pm 25\%$ for $n = 1, 3, 7$; this ratio almost does not change for harmonic $n = 5$ in our example for $k = 2.1$ (compare Fig. 3 with Fig. 4); this agrees with the results in Fig. 1. The power variation for high harmonics with $n > 7$ can be $\sim 300\%$, but they remain rather weak. Odd harmonics are very weak.

In Fig. 5 we demonstrate the shape of the periodic magnetic field with harmonics. The third undulator field harmonic with negative phase, $d < 0$, increases the amplitude of the magnetic field (see Fig. 5). For $d > 0$, the amplitude of the magnetic field may even decrease (see Fig. 5).

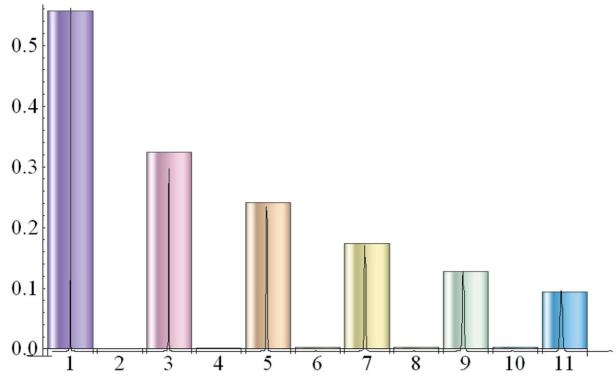

Figure 4
Spontaneous UR harmonic intensity (in relative units) from the undulator with $k = 2.1$, $h = 3$, $d = -0.42$, $\sigma_e = 1.5 \times 10^{-3}$ for the harmonic number n.

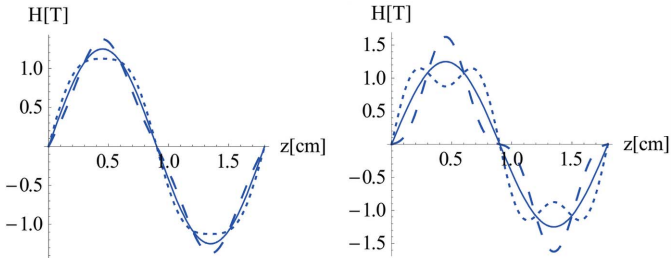

Figure 5
The undulator magnetic field for $k = 2.1$, $h = 3$, $d = \pm 0.1$ (left plot), $d = \pm 0.42$ (right plot), $d = 0$ (solid lines), $d > 0$ (dotted lines), $d < 0$ (dashed lines).

3. Phenomenological description of FEL harmonics evolution

The analytical formulation of the power evolution in a single-pass FEL was developed by Dattoli and co-workers (Dattoli & Ottaviani, 2002; Dattoli *et al.*, 2004, 2005*a*,*b*); it employs the logistic function. The model was improved and calibrated with FEL experiments by Zhukovsky and co-workers (Zhukovsky & Potapov, 2017; Zhukovsky, 2017*a*,*b*, 2018; Zhukovsky & Kalitenko, 2019*a*,*b*). In the following we present its development, which describes high harmonic growth around the saturated region. The Pierce parameter for the nth FEL harmonic (Dattoli *et al.*, 2005*b*) reads as follows,

$$\rho_n = \frac{J^{1/3}(\lambda_u k f_n)^{2/3}}{2\gamma(4\pi i)^{1/3}}, \quad \tilde{\rho}_n = \frac{\rho_n}{\left(1+\mu_{D,n}\right)^{1/3}}, \quad \mu_{D,n} \cong \frac{\lambda_u \lambda_n}{16\pi\rho_n \Sigma}, \tag{8}$$

where accounting for diffraction comes through the beam section $\Sigma = 2\pi(\beta_x \varepsilon_x \beta_y \varepsilon_y)^{1/2}$ for harmonic wavelength λ_n and undulator period λ_u; J is the current and f_n is the Bessel coefficient. The corrected gain length is $L_{n,g} \cong \Phi_n \lambda_u / 4\pi\sqrt{3} n^{1/3} \tilde{\rho}_n$, the saturation occurs at $L_s \cong 1.07 L_{1,g} \ln(9\eta_1 P_F / P_{1,0})$, the saturated harmonic powers are $P_F \cong \sqrt{2} P_e \eta_1 \tilde{\rho}_1^2 / \rho_1$, $P_{n,F} = \eta_n P_F f_n^2 / n^{5/2} f_1^2$ and P_e is the electron beam power. The following phenomenological corrections account for the beam size and the energy spread σ_e,

$$\eta_n \cong \left\{ \exp\left[-\Phi_n(\Phi_n - 0.9) \right] + 1.57(\Phi_n - 0.9)/\Phi_n^3 \right\} / 1.062, \tag{9}$$

$$\Phi_n \cong \left(\zeta^n + 0.165\mu_{\varepsilon,n}^2\right) \exp\left(0.034\mu_{\varepsilon,n}^2\right), \quad \mu_{\varepsilon,n}(\sigma_\varepsilon) \cong 2\sigma_\varepsilon / n^{1/3} \tilde{\rho}_n, \tag{10}$$

$$\zeta \cong 1 + 0.07 \sum_i \mu_i + 0.35 \sum_i \mu_i^2, \tag{11}$$

$$\mu_{\tilde{x},\tilde{y}} = \frac{1}{\tilde{\rho}} \frac{\gamma^2 \varepsilon_{x,y}}{(1 + k^2/2)\lambda_u \beta_{x,y}}, \quad \mu_{x,y} = \frac{1}{\tilde{\rho}} \frac{\gamma^2 \omega_\beta^2 \varepsilon_{x,y}}{(1 + k^2/2)\gamma_{x,y}}, \tag{12}$$

where $\varepsilon_{x,y}$ are the emittances, $\beta_{x,y}$ and $\gamma_{x,y}$ are the Twiss parameters, $\omega_\beta = \pi k / \gamma \lambda_u$ is the betatron frequency, $\tilde{\rho}_n < \rho$ by ~ 15–30%, $\zeta \simeq 1$–1.05. The conditions for stable amplifi-

cation (McNeil & Thompson, 2010; Pellegrini *et al.*, 2016; Huang & Kim, 2007; Saldin *et al.*, 2000) are $\sigma_\varepsilon \leq \tilde{\rho}_n/2$, $\varepsilon_{x,y} \leq \lambda_n/4\pi$. The radiation power exponentially grows along the FEL; for the initially unbunched beam it reads (Dattoli *et al.*, 2004, 2005*a*,*b*) as follows,

$$P_{L,n}(z) \cong \frac{P_{0,n}\, A(n,z)\exp(0.223z/Z_s)}{1+[A(n,z)-1]P_{0,n}/P_{n,F}}, \quad (13)$$

$$A(n,z) \cong \frac{1}{3}+\frac{\cosh(z/L_{n,g})}{4.5}+\frac{\cos(\sqrt{3}z/2L_{n,g})\cosh(z/2L_{n,g})}{0.444},$$

where $P_{0,n}$ is the initial power for the nth harmonic. The nonlinear power term, induced by the fundamental tone, is (Dattoli *et al.*, 2005*b*)

$$Q_n(z) \cong P_{n,0}\frac{\exp\left(n\,z/L_g\right)}{1+\left[\exp\left(n\,z/L_g\right)-1\right]P_{n,0}/P_{n,F}}, \quad (14)$$

where $P_{n,0} \cong b_n^2\, P_{n,F}$ is the equivalent initial power due to the induced bunching $b_n^2 \cong (P_{0,1}/9P_e\,\tilde{\rho}_1)^n$. The power evolution in sectioned undulators, the bunching coefficients, energy spread and other details can be found elsewhere (Dattoli *et al.*, 2005*a*,*b*, 2017*a*,*b*, 2018; Zhukovsky & Potapov, 2017; Zhukovsky & Kalitenko, 2019*a*).

Equations (13) and (14) though do not describe the harmonic evolution close to saturation. In reality the harmonic power saturates gradually, while the sum of (13) and (14) describes the saturation in one step. To address multi-stage harmonic saturation we introduce another broadening coefficient, $\tilde{\mu}_{\varepsilon,n}(\sigma_\varepsilon) \cong 2n\sigma_\varepsilon/(n^{1/3}\tilde{\rho}_n)$, which involves an additional factor n to describe higher losses for high UR harmonics and their spectrum line broadening in accordance with Zhukovsky (2015*a*,*b*, 2016*b*). This yields other broadening coefficients,

$$\tilde{\eta}_n \cong \left\{\exp\left[-\tilde{\Phi}_n\left(\tilde{\Phi}_n-0.9\right)\right]+1.57\left(\tilde{\Phi}_n-0.9\right)/\tilde{\Phi}_n^3\right\}/1.062, \quad (15)$$

$$\tilde{\Phi}_n \cong \left(\zeta^n+0.165\tilde{\mu}_{\varepsilon,n}^2\right)\exp\left(0.034\tilde{\mu}_{\varepsilon,n}^2\right),$$
$$\tilde{\mu}_{\varepsilon,n}(\sigma_\varepsilon) \cong 2n^{2/3}\sigma_\varepsilon/\tilde{\rho}_n. \quad (16)$$

They in turn modify the power values $\tilde{P}_{n,F} = \tilde{\eta}_n\tilde{P}_F f_n^2/n^{5/2}f_1^2$, $\tilde{P}_F \cong \sqrt{2}P_e\tilde{\eta}_1\tilde{\rho}_1^2/\rho_1$, $\tilde{P}_{n,0} \cong d_n b_n^2\tilde{P}_{n,F}$ and the gain length $\tilde{L}_{n,g} \cong \tilde{\Phi}_n\lambda_u/4\pi\sqrt{3}n^{1/3}\tilde{\rho}_n$; the coefficients $d_n \cong \{1, 3, 8, 40, 120\}$ describe the anticipated harmonic power growth up to the first stage of saturation. A new nonlinear term appears,

$$\tilde{Q}_n(z) \cong \tilde{P}_{n,0}\frac{\exp\left(n\,z/L_g\right)}{1+\left[\exp\left(n\,z/L_g\right)-1\right]\tilde{P}_{n,0}/\tilde{P}_{n,F}}, \quad (17)$$

which should be taken into account together with (14). The results of the modeling with (8)–(17) are presented in the following section. The phenomenological model is flexible: intersectional losses, imposed by harmonic filtering or phase shifters, can be introduced *etc*. It can be easily implemented in any computer program, such as *Mathematica*, and it allows instant analysis of FELs.

4. Effect of the third field harmonic on the planar FEL radiation

Using our new formulation of the total FEL power, $P_{L,n}+Q_n+\tilde{Q}_n$, we modeled several well documented FEL experiments; below we present some examples, comparisons with the measurements and numerical simulations. We modeled an LCLS experiment, where the radiation at λ_1 = 0.15 nm was produced in the FEL, built with 17 undulators, each 3.4 m long, with 15 cm gaps between them, k = 3.5, λ_u = 3 cm. The electron energy was E = 13.6 GeV, the energy spread $\sigma_e = 1\times10^{-4}$, the emittance $\varepsilon_{x,y}$ = 0.4 µm rad [see Emma *et al.* (2010) for details]. The saturated power in our model was ≃20 GW, the gain length L_g = 3.7 m, the saturation length $L_s \simeq$ 56.5 m of pure undulators; $L_s \simeq$ 60 m, including the gaps. The measurements (Ratner *et al.*, 2011) gave the power rate of high harmonics as 0.2 to <2% of the fundamental, which included all high harmonic contributions. The fifth harmonic power was estimated at ∼0.1 of the power of the third harmonic; the second harmonic was not registered in the experiment. Our modeling results and the experimental values agree very well.

Soft X-rays, λ_1 = 1.5 nm, were produced in the LCLS experiment for E = 4.3 GeV, I_0 = 1 kA, $\sigma_e = 3\times10^{-4}$, $\varepsilon_{x,y}$ = 0.4 mm mrad. In this case the measured power of the third harmonic was 2–3% of the fundamental, the fifth harmonic was estimated at ∼0.1 of the third harmonic power and the second harmonic power was <0.1%. A comparison of the results of our modeling with the experimental range is presented in Fig. 6. The harmonic powers are within or close to the experimental range, denoted by the shadowed areas on the right in Fig. 6. The effect of the third undulator field harmonic on the radiated UR harmonics is shown in Fig. 6, where we omitted the noise contribution to show pure power growth. Note the four-stage evolution of the harmonic powers, described by our model: the lethargy region <5 m is followed by the independent harmonic growth (13), after 15 m the nonlinear generation (17) develops until the first saturation at

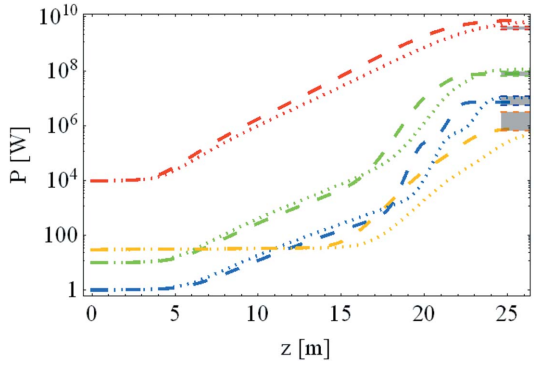

Figure 6
Effect of the third undulator field harmonic on the FEL power in the low-energy LCLS experiment with E = 4.3 GeV, I_0 = 1 kA, $\sigma_e = 3\times10^{-4}$, $\varepsilon_{x,y}$ = 0.4 mm mrad, β = 15 m, λ_u = 3 cm, k = 3.5. Modeled power for harmonics: n = 1 (red), n = 2 (orange), n = 3 (green), n = 5 (blue); d = −0.3 (dashed lines), d = +0.3 (dotted lines). The experimental saturated power range for harmonics is denoted by shadowed areas.

$\sim$20 m, and then the growth still proceeds (14) until the final saturation power is reached.

For $d = -0.3$ (dashed lines in Fig. 6) we obtained some shorter gain and saturation lengths, a slightly stronger fundamental and slightly weaker high harmonics. For $d = +0.3$ (dotted lines in Fig. 6), the effect was the opposite. It was noticeable more for the gain length than for the saturated harmonic powers, although the latter changed by $\sim$25%. The second FEL harmonic was much weaker than the fifth, though its saturated power was higher than the initial power of the fundamental tone.

In the LEUTL FEL experiment (Milton *et al.*, 2001) the radiation at $\lambda_1 = 385$ nm was produced by the current $I_0 = 184$ A of electrons with $\gamma = 500$. Our modeling agrees well with the experimental results: the saturation power 0.1 GW, length $L_s \simeq 15$ m and gain $L_g = 0.8$ m are all well reproduced. The harmonic powers reach saturation in two stages and stay within the experimental range. The effect of the third field harmonic is similar to that in Fig. 6 and we omit it for brevity.

Similarly good was the match with the SPARC experiment (Giannessi *et al.*, 2011), where quite low energy electrons with $\gamma = 297$ emitted radiation at 0.5 μm. The phenomenological modeling yields a pure undulator FEL length $L_s = 13.3$ m and $L_g = 0.64$ m; this agrees with the measurements of Giannessi *et al.* (2011), with *GENESIS* numerical simulations by Alesini *et al.* (2004) and with our own numerical simulations. Details of the above examples are given by Zhukovsky (2019).

We modeled FEL experiments at the SPring-8 X-ray source in its upgraded (Owada *et al.*, 2018) and original (Shintake *et al.*, 2009) setups. The FEL power evolution in the SACLA FEL experiment (Owada *et al.*, 2018) with the current $I = 120$ A, $\gamma = 1570$, $\sigma_e = 3 \times 10^{-4}$, $\varepsilon_{x,y}^n = 1$ mm mrad, $\lambda_u = 1.8$ cm, $k = 2.1$ is shown in Fig. 7. We obtained a gain length $L_g = 1$ m and saturation length $L_s = 12.7$ m, as reported by Owada *et al.* (2018); the harmonic powers for the radiation at $\lambda_1 = 12$ nm, $\lambda_3 = 4$ nm, $\lambda_5 = 2.4$ nm are $P_{F,n} \simeq 1 \times 10^8, 1 \times 10^6, 8 \times 10^4$ W. The rate $P_{F,3}/P_{F,1} \simeq 0.9\%$ agrees quite well with the 0.5% reported by Owada *et al.* (2018) as well as $P_{F,5}/P_{F,3} \simeq 7\%$. The effect of the third undulator field harmonic with $d = \pm 0.3$ in

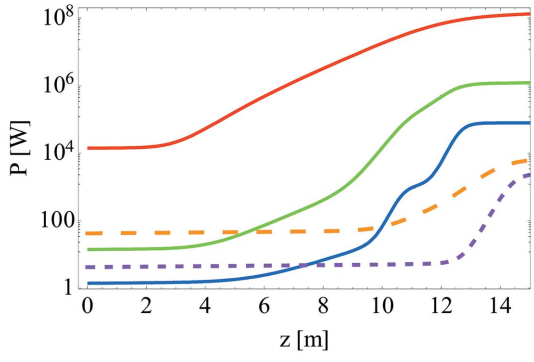

Figure 7
FEL harmonic power evolution in the SACLA FEL experiment with $I = 120$ A, $\gamma = 1570$, $\sigma_e = 3 \times 10^{-4}$, $\varepsilon_{x,y}^n = 1$ mm mrad, $\lambda_u = 1.8$ cm, $k = 2.1$. Harmonics: $n = 1$ (red), $n = 3$ (green), $n = 5$ (blue), $n = 2$ (orange dashed), $n = 4$ (violet dotted).

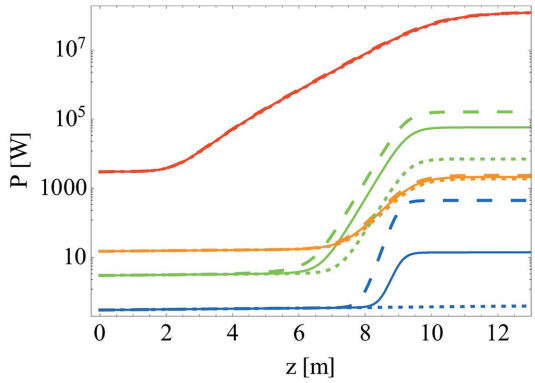

Figure 8
FEL harmonic power evolution in the SPring-8 FEL experiment with $I = 300$ A, $\gamma = 489$, $\sigma_e = 2 \times 10^{-4}$, $\varepsilon_{x,y}^n = 2.7$ mm mrad, $\lambda_u = 1.5$ cm, $k = 0.7$. Harmonics: $n = 1$ (red), $n = 3$ (green), $n = 5$ (blue), $n = 2$ (orange). $d = 0$ (solid lines), $d = -0.3$ (dashed lines), $d = 0.3$ (dotted lines).

(1) on the FEL radiation was insignificant in this experimental setup; it has been omitted in Fig. 7.

In SPring-8 installations the undulator parameter k varies over a wide range. We modeled another experimental setup (Shintake *et al.*, 2009) with $k = 0.7$, $\lambda_u = 1.5$ cm, $I = 300$ A, $\gamma = 489$, $\sigma_e = 2 \times 10^{-4}$, $\varepsilon_{x,y}^n = 2.7$ mm mrad, $\lambda_1 = 39$ nm, $\lambda_3 = 13$ nm, $\lambda_5 = 8$ nm (see the FEL power in Fig. 8).

In Fig. 8, solid lines describe radiated harmonics from the FEL undulator with an ideal sinusoidal field, $d = 0$. The additional third undulator field harmonic strongly influences the FEL harmonic powers in this setup (see Fig. 8). The third FEL harmonic power reaches 160 kW for $d = -0.3$, 55 kW for $d = 0$, and just 7 kW for $d = 0.3$; the variation is $\sim$200%. The fifth FEL harmonic is weak; it does not develop for $d = 0.3$ and it reaches 0.5 kW for $d = -0.3$. The first and second harmonics are almost not affected (see Fig. 8).

5. Effect of the third field harmonic on the elliptic FEL radiation

In some elliptic undulators the harmonics of the undulator magnetic field can be significant. Lee *et al.* (2015) studied a bi-harmonic undulator numerically; the amplitude of the main undulator field was 9.7 kG and the amplitude of the third field harmonic was 0.8 kG. The magnetic field in the undulator was

$$\mathbf{H} = H_0 \begin{bmatrix} \sin(k_\lambda z) - d\sin(hk_\lambda z) \\ \cos(k_\lambda z) + d\cos(hk_\lambda z) \\ 0 \end{bmatrix}, \qquad (18)$$

the undulator period was $\lambda = 2.3$ cm, $k = 2.21622$, $h = 3$, $d = 0.0825$. The wavelength of the UR from the undulator with the field (18) is given by (6), where $k_{\rm eff}^2 = k^2[1 + (d^2/h^2)]$. We have performed rigorous analytical calculations and obtained the Bessel functions for this undulator. The radiation integral for the undulator field (18) yields the following generalized Bessel functions,

$$J_n^h(\xi_1,\xi_2,\xi_3,\xi_4,\xi_5)=\frac{1}{2\pi}\int_{-\pi}^{\pi}\mathrm{d}\alpha\exp\Big(i\Big\{n\alpha+\xi_1\cos\alpha+\xi_2\cos(h\alpha)-\xi_3\sin\alpha+\xi_4\sin(h\alpha)-\xi_5\sin[(h+1)\alpha]\Big\}\Big),\quad(19)$$

$$\xi_1=\frac{2nk\gamma\theta\cos\phi}{1+k^2\big[1+(d/h)^2+\gamma^2\theta^2\big]},$$
$$\xi_2=\frac{d}{h^2}\,\xi_1,\quad \xi_3=\xi_1\tan\phi,\quad \xi_4=\frac{d}{h^2}\,\xi_1\tan\phi,\quad(20)$$
$$\xi_5=\frac{2ndk^2}{h(h+1)\big\{1+k^2\big[1+(d/h)^2+\gamma^2\theta^2\big]\big\}}.$$

The UR intensity is given by (7), where $k_{\rm eff}^2=k^2\big[1+(d^2/h^2)\big]$. The generalized Bessel functions (19) yield the following amplitudes for the spontaneous UR in the angle θ off the axis,

$$T_{n;x}=\frac{2\gamma}{k}\theta\cos\phi\,J_n^h+i\big(J_{n+1}^h-J_{n-1}^h\big)+i\frac{d}{h}\big(J_{n+1}^h-J_{n-h}^h\big),\quad(21)$$

$$T_{n;y}=\frac{2\gamma}{k}\,\theta\sin\phi\,J_n^h-\big(J_{n+1}^h+J_{n-1}^h\big)+\frac{d}{h}\big(J_{n+h}^h+J_{n-h}^h\big).\quad(22)$$

The intensities of the spontaneous UR in the undulator (18) with the data taken from Lee *et al.* (2015) are shown in Fig. 9 for $d=0.0825$ and $d=0.3$ in the upper and lower plots, respectively.

The second harmonic is evident in the UR spectrum; its power is 8.7% of the fundamental tone; ideally, only the first harmonic should be radiated by the helical undulator on the axis. Note also that the fifth harmonic is stronger than the third; this is due to the third undulator field harmonic with amplitude d in (18). For $d=0.3$ its power is 15.5% of the fundamental (see lower plot in Fig. 9). The Bessel coefficients are $f_{n;x,y}=|T_{n;x,y}|$. On the undulator axis $\theta=0$, only the ξ_5 argument survives in $J_n^h(\xi_i)$ and we obtain (21) and (22) with $J_n^h(\xi_5)=\int_{-\pi}^{\pi}\mathrm{d}\alpha\exp(i\{n\alpha-\xi_5\sin[(h+1)\alpha]\})/2\pi$. For $d=0$ we obtain a common result for the spiral undulator: $f_{1;x,y}=1$ and $f_{n\neq1}=0$.

We have applied the phenomenological FEL model to describe the evolution of the harmonic power in the FEL with the bi-harmonic helical undulator (18). We considered the beam of the LCLS installation with the low-energy value, $E=4.3$ GeV, and the SACLA beam with $E=800$ MeV, where the planar undulator with close value of k was employed. The modeling data are the following: $\gamma=8400$, $P_{\rm E}=4292$ GW, $J=2.23\times10^{11}$ A, $\Sigma_{\rm beam}=4.49\times10^{-9}$ m^2, $I_0=1$ kA, $\sigma_{\rm e}=0.0003$, $\varepsilon^n=0.4\times10^{-6}$ μm rad, $\beta=15$ m, $\zeta=1.05$, $k=2.21622$, $h=3$, $\lambda_{\rm u}=2.3$ cm, $L_{\rm s}=24.5$ m, $L_{\rm g}=1.5$ m, $\lambda_1=0.97$ nm, $\lambda_2=0.49$ nm, $\lambda_3=0.32$ nm, $\lambda_4=0.24$ nm, $\lambda_5=0.19$ nm.

For $d=0.3$,

$$f_{n;y,x}=\{0.9958,0.0550,0.0380,0.0162,0.0984\},$$
$$\rho_{n;y,x}\simeq\{0.00080,0.00011,0.00008,0.00005,0.00017\},$$
$$P_{n,y,x,F}\simeq\{4.4\times10^9,44.3\times10^3,4.41\times10^3,4.4,211\times10^3\}\ \text{W}.$$

For $d=0.08247$,

$$f_{n;y,x}=0.9980,0.0557,0.0109,0.0047,0.0275,$$
$$\rho_{n;y,x}\simeq\{0.00080,0.00011,0.00003,0.00002,0.00007\},$$
$$P_{n,y,x,F}\simeq\{4.45\times10^9,47.3\times10^3,0,04,560\}\ \text{W}.$$

The simulations of the FEL power evolution along the undulators for $d=0.08247$ and for $d=0.3$ are shown in Fig. 10.

The power of the fundamental FEL harmonic is the same for x- and y-polarizations: ∼4 GW. Note in Fig. 10 that the powers of the high harmonics are rather weak, but for the fifth

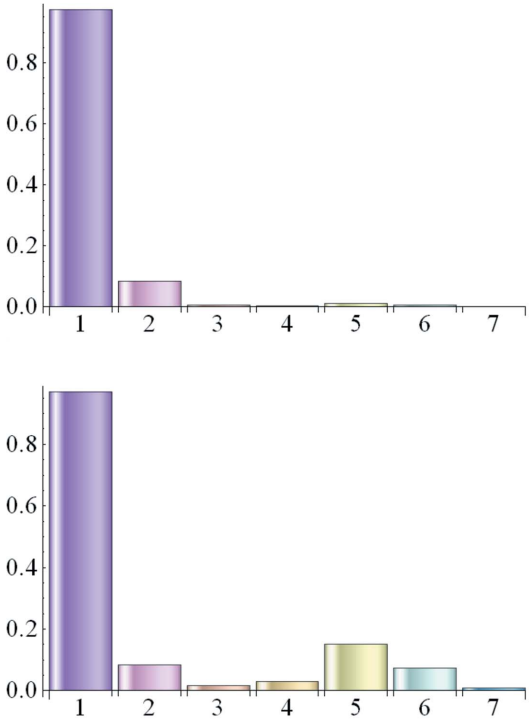

Figure 9
Spontaneous UR harmonic intensity in the undulator (18) for $h=3$, $d=0.0825$ (top plot) and $d=0.3$ (bottom plot) (in relative units).

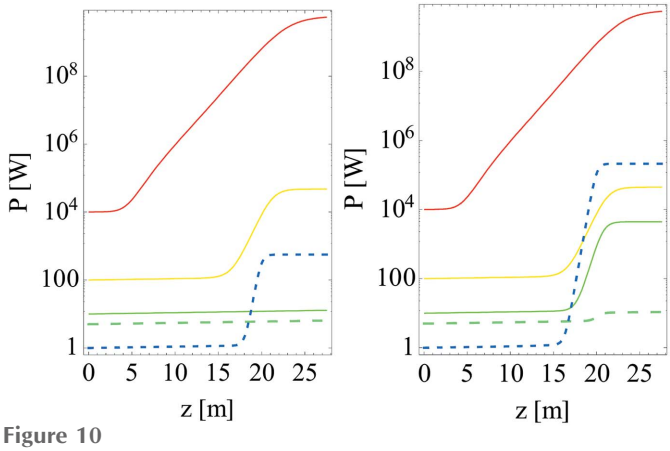

Figure 10
Harmonic power evolution in the cos–sin spiral undulator FEL with the field (18) for $\gamma=1570$, $I_0=120$ A, $\varepsilon^n=10^{-6}$ mm mrad, $\beta=0.37$ m, $k=2.216$, $h=3$, $\lambda_{\rm u}=2.3$ cm; both x- and y-polarization have the same power. Harmonics: $n=1$ (red), $n=2$ (yellow), $n=3$ (green), $n=4$ (green dashed), $n=5$ (blue dotted). Undulator with $d=0.0824742$ (left plot) and $d=0.3$ (right plot).

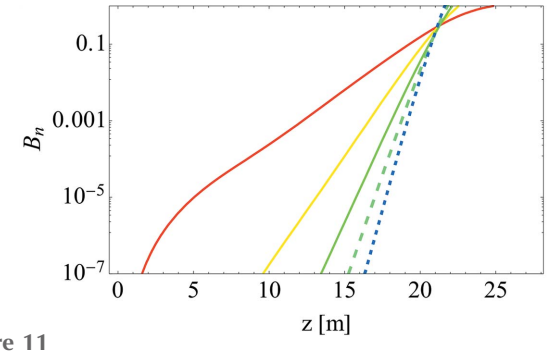

Figure 11
Bunching evolution in the cos–sin spiral undulator FEL with the field (18) for $\gamma = 1570$, $I_0 = 120$ A, $\varepsilon^n = 10^{-6}$ mm mrad, $\beta = 0.37$ m, $k = 2.216$, $h = 3$, $d = 0.3$, $\lambda_u = 2.3$ cm. Harmonics: $n = 1$ (red), $n = 2$ (yellow), $n = 3$ (green), $n = 4$ (green dashed), $n = 5$ (blue dotted).

harmonic the power reaches 0.2 MW for $d = 0.3$ and 0.5 kW for $d = 0.08247$. The second harmonic has a power of ∼45 kW. It is evident upon comparison of the plots in Fig. 10 that the third and the fifth FEL harmonics are stronger in the undulator (18) for higher values of d, *i.e.* for stronger undulator field harmonics. The bunching evolution, corresponding to the FEL power evolution in the right-hand plot in Fig. 10, is demonstrated in Fig. 11.

We also studied the radiation from the FEL with the bi-harmonic elliptic undulator (18) and SACLA installation beam. Assuming SACLA standard focusing, $\beta = 5$ m, the second harmonic is quite weak (see Fig. 12); the fifth FEL harmonic is weak, but it is amplified due to the third undulator field harmonic [see (18)], especially for $d = 0.3$ (see blue dotted lines in Figs. 12 and 10). The modeling data for the FEL with the SACLA beam and the undulator (18) for $d = 0.08247$ are as follows: $\gamma = 1570$, $P_E = 96.27$ GW, $J = 6 \times 10^9$ A, $\Sigma_{beam} = 2 \times 10^{-8}$ m^2, $I_0 = 120$ A, $\sigma_e = 0.0002$, $\varepsilon^n = 10^{-6}$ μm rad, $\beta = 5$ m, $\zeta = 1.05$, $k = 2.21622$, $h = 3$, $d = 0.08247$, $\lambda_u = 2.3$ cm, $L_s = 11.8$ m, $L_g = 0.97$ m, $\lambda_1 = 27.6$ nm, $\lambda_2 = 13.8$ nm, $\lambda_3 = 9.2$ nm, $\lambda_4 = 6.90$ nm, $\lambda_5 = 5.52$ nm,

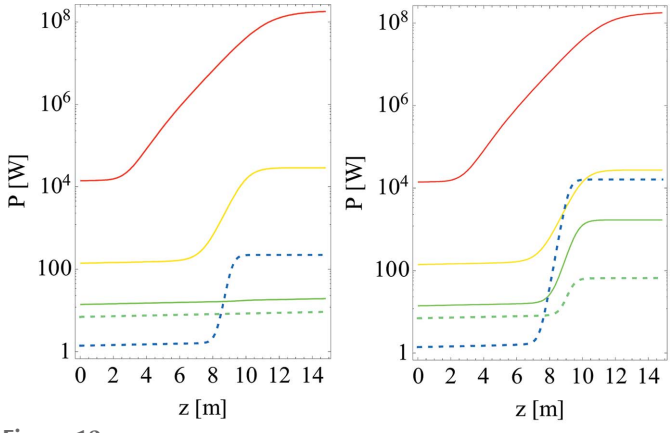

Figure 12
Harmonic power evolution in the cos–sin elliptic undulator FEL with the field (18) for the SACLA beam: $\beta = 5$ m, $k = 2.21622$, $h = 3$, $\lambda_u = 2.3$ cm; both x- and y-polarization have the same power. Harmonics: $n = 1$ (red), $n = 2$ (yellow), $n = 3$ (green), $n = 4$ (green dashed), $n = 5$ (blue dotted). Undulator with $d = 0.0824742$ (left plot) and $d = 0.3$ (right plot).

$$f_{n;y,x} = \{0.9974, 0.0657, 0.0113, 0.0056, 0.0271\},$$
$$\rho_{n;y,x} \simeq \{0.00117, 0.00016, 0.00004, 0.000025, 0.00009\},$$
$$P_{n,y,x,F} \simeq \{1.37 \times 10^8, 28.7 \times 10^3, 0.8, 0, 220\} \text{ W}.$$

The gain length of the considered bi-harmonic elliptic FEL is $L_g \simeq 1$ m and the saturation length is $L_s \simeq 12$ m independent of d. The saturated power of the fundamental tone reaches 0.14 GW. Already for $d \simeq 0.08$ the fifth UR harmonic gets some boost (see left-hand plot in Fig. 12); for $d = 0.3$ its power exceeds 10 kW and the third UR harmonic appears (see right-hand plot in Fig. 12). Thus, a relatively weak third undulator field harmonic with $d \simeq 0.1$–0.3 and off-axis effects can generate noticeable second and fifth UR harmonics of the spontaneous and stimulated radiation. The effect of the undulator field harmonic is stronger on the spontaneous UR than on the FEL radiation. The fifth UR harmonic is stronger than the third.

6. Conclusions

We analyzed the influence of the third harmonic of the undulator field on the spontaneous and stimulated radiation for planar and elliptic undulators. We obtained exact analytical expressions for the Bessel coefficients. They depend on the undulator parameter k and on the third field harmonic rate d in (1) and in (18). For the planar undulator we found that if $k < 1.5$ then the third field harmonic with $d < 0$ (negative phase) enhances UR harmonics with $n = 3, 5, \ldots$, and for $d > 0$ (positive phase) the power of the high harmonics decreases (see Fig. 1). If $k > 1.5$, then the effect of the magnetic field harmonic in (1) is the opposite: high UR harmonics $n = 3, 5, \ldots$ are stronger for $d > 0$ and weaker for $d < 0$ (see Fig. 1). This observation corrects and clarifies previous reports in the literature (Zhukovsky, 2015*a*,*b*, 2016*a*,*b*; Jeevakhan & Mishra, 2011; Mishra *et al.*, 2009; Jia, 2011).

The effect of the energy spread $\sigma_e \simeq 10^{-4}$ on the UR is small; for $\sigma_e \simeq 10^{-3}$, high UR harmonic power decreases as expected (see Fig. 2). All of the above results were confirmed by numerical simulations using the *SPECTRA* program: see Figs. 3 and 4.

We further developed the phenomenological FEL model, including the description of the harmonic behavior around the saturation region and the multi-stage saturation, which matches the experiments. We studied the harmonic generation in several setups of SPring-8, SACLA and LCLS FEL installations. Our modeling (see Fig. 7) agreed with the experimental measurements, with our numerical simulations in *PERSEO* (Zhukovsky & Kalitenko, 2019*c*,*d*) and with the results using the *GENESIS* program. The match for the third and fifth harmonic powers was remarkably good. The second harmonic power had fairly good agreement with the experiments too.

We explored the influence of the third undulator field harmonic on the FEL radiation. For a planar undulator with $k \simeq 2$ the effect is small for any d; for $k \simeq 3.5$ it is noticeable for $d = \pm 0.3$. For $k \simeq 1$ and, in particular, for $k < 1$, the effect

of the second field in (1) can be significant. We studied the SPring-8 FEL with $\gamma = 489$, $\sigma_e = 2 \times 10^{-4}$, $\varepsilon_{x,y}^{n} = 2.7$ mm mrad, $k = 0.7$, $\lambda_u = 1.5$ cm, $I = 300$ A, fundamental wavelength $\lambda_1 = 40$ nm (Shintake *et al.*, 2009); the change of the power of the third harmonic is $\sim$200% for $d = \pm 0.3$ (see Fig. 8). The change of the harmonic power for $n = 5$ can be $\sim 10^2$ times (see Fig. 8). The second FEL harmonic is influenced mostly by the finite beam size and off-axis effect. The newly updated SACLA setup is not sensitive to the third undulator field harmonic.

We studied the third field harmonic effect in an elliptic undulator (18). Even a relatively weak third undulator field harmonic, $d \simeq 0.08$, in (18) gives rise to a noticeable fifth UR harmonic (see Figs. 9 and 10). The fifth UR harmonic is stronger than the third. Their powers further increase by two orders of magnitude if $d = 0.3$. Due to the finite electron beam size and divergence, the radiation of the second harmonic can be significant; it can prevail over the fifth harmonic, whose content is $\sim$0.01% (see Fig. 12).

The above analysis may help to identify the degree of harmonic presence in FEL radiation, attributed to the undulator field harmonics.

Acknowledgements

We are grateful to Professor A. V.Borisov for useful notes and to A. M. Kalitenko for the *SPECTRA* data and his help in checking some of the Bessel functions.

References

Alesini, D., Bertolucci, S., Biagini, M. E., Biscari, C., Boni, R., Boscolo, M., Castellano, M., Clozza, A., Di Pirro, G., Drago, A., Esposito, A., Ferrario, M., Fusco, V., Gallo, A., Ghigo, A., Guiducci, S., Incurvati, M., Ligi, C., Marcellini, F., Migliorati, M., Milardi, C., Mostacci, A., Palumbo, L., Pellegrino, L., Preger, M., Raimondi, P., Ricci, R., Sanelli, C., Serio, M., Sgamma, F., Spataro, B., Stecchi, A., Stella, A., Tazzioli, F., Vaccarezza, C., Vescovi, M., Vicario, C., Zobov, M., Alessandria, F., Bacci, A., Boscolo, I., Broggi, F., Cialdi, S., DeMartinis, C., Giove, D., Maroli, C., Mauri, M., Petrillo, V., Romè, M., Serafini, L., Levi, D., Mattioli, M., Medici, G., Catani, L., Chiadroni, E., Tazzari, S., Bartolini, R., Ciocci, F., Dattoli, G., Doria, A., Flora, F., Gallerano, G. P., Giannessi, L., Giovenale, E., Messina, G., Mezi, L., Ottaviani, P. L., Pagnutti, S., Picardi, L., Quattromini, M., Renieri, A., Ronsivalle, C., Cianchi, A., Angelo, A. D., Di Salvo, R., Fantini, A., Moricciani, D., Schaerf, C. & Rosenzweig, J. B. (2004). *Nucl. Instrum. Methods Phys. Res. A*, **528**, 586–590.
Dattoli, G., Giannessi, L., Ottaviani, P. L. & Ronsivalle, C. (2004). *J. Appl. Phys.* **95**, 3206–3210.
Dattoli, G. & Ottaviani, P. L. (2002). *Opt. Commun.* **204**, 283–297.
Dattoli, G., Ottaviani, P. L. & Pagnutti, S. (2005*b*). *J. Appl. Phys.* **97**, 113102.
Dattoli, G., Ottaviani, P. L. & Renieri, A. (2005*a*). *Laser Part. Beams*, **23**, 303.
Emma, P. *et al.* (2010). *Nat. Photon.* **4**, 641–647.
Giannessi, L. *et al.* (2011). *Phys. Rev. ST Accel. Beams*, **14**, 060712.
Huang, Z. & Kim, K.-J. (2007). *Phys. Rev. ST Accel. Beams*, **10**, 034801.
Jeevakhan, H. & Mishra, G. (2011). *Nucl. Instrum. Methods Phys. Res. A*, **656**, 101–106.
Jia, Q. (2011). *Phys. Rev. ST Accel. Beams*, **14**, 060702.
Lee, K., Mun, J., Hee Park, S., Jang, K., Uk Jeong, Y. & Vinokurov, N. A. (2015). *Nucl. Instrum. Methods Phys. Res. A*, **776**, 27–33.
McNeil, B. W. J. & Thompson, N. R. (2010). *Nat. Photon.* **4**, 814–821.
Margaritondo, G. & Rebernik Ribic, P. (2011). *J. Synchrotron Rad.* **18**, 101–108.
Milton, S. V., Gluskin, E., Arnold, N. D., Benson, C., Berg, W., Biedron, S. G., Borland, M., Chae, Y. C., Dejus, R. J., Den Hartog, P. K., Deriy, B., Erdmann, M., Eidelman, Y. I., Hahne, M. W., Huang, Z., Kim, K. J., Lewellen, J. W., Li, Y., Lumpkin, A. H., Makarov, O., Moog, E. R., Nassiri, A., Sajaev, V., Soliday, R., Tieman, B. J., Trakhtenberg, E. M., Travish, G., Vasserman, I. B., Vinokurov, N. A., Wang, X. J., Wiemerslage, G. & Yang, B. X. (2001). *Science*, **292**, 2037–2041.
Mishra, G., Gehlot, M. & Hussain, J. K. (2009). *Nucl. Instrum. Methods Phys. Res. A*, **603**, 495–503.
Owada, S., Togawa, K., Inagaki, T., Hara, T., Tanaka, T., Joti, Y., Koyama, T., Nakajima, K., Ohashi, H., Senba, Y., Togashi, T., Tono, K., Yamaga, M., Yumoto, H., Yabashi, M., Tanaka, H. & Ishikawa, T. (2018). *J. Synchrotron Rad.* **25**, 282–288.
Pellegrini, C. (2016). *Phys. Scr.* T**169**, 014004.
Pellegrini, C., Marinelli, A. & Reiche, S. (2016). *Rev. Mod. Phys.* **88**, 015006.
Ratner, D., Brachmann, A., Decker, F. J., Ding, Y., Dowell, D., Emma, P., Fisher, A., Frisch, J., Gilevich, S., Huang, Z., Hering, P., Iverson, R., Krzywinski, J., Loos, H., Messerschmidt, M., Nuhn, H. D., Smith, T., Turner, J., Welch, J., White, W. & Wu, J. (2011). *Phys. Rev. ST Accel. Beams*, 14, 060701.
Saldin, E. L., Schneidmiller, E. A. & Yurkov, M. V. (2000). *The Physics of Free Electron Lasers.* Springer.
Shintake, T. *et al.* (2009). *Phys. Rev. ST Accel. Beams*, **12**, 070701.
Tanaka, T. (2014). *Phys. Rev. ST Accel. Beams*, **17**, 060702.
Tanaka, T. & Kitamura, H. (2001). *J. Synchrotron Rad.* **8**, 1221–1228.
Zhukovsky, K. V. (2015*a*). *Moscow Univ. Phys.* **70**, 232–239.
Zhukovsky, K. (2015*b*). *Opt. Commun.* **353**, 35–41.
Zhukovsky, K. (2016*a*). *Laser Part. Beams* **34**, 447.
Zhukovsky, K. (2016*b*). *Nucl. Instrum. Methods Phys. Res. B*, **369**, 9–14.
Zhukovsky, K. (2017*a*). *J. Phys. D Appl. Phys.* **50**, 505601.
Zhukovsky, K. J. (2017*b*). *J. Appl. Phys.* **122**, 233103.
Zhukovsky, K. V. (2018). *Russ. Phys. J.* **60**, 1630–1637.
Zhukovsky, K. V. (2019). *Results Phys.* **13**, 102248.
Zhukovsky, K. & Kalitenko, A. (2019*a*). *J. Synchrotron Rad.* **26**, 159–169.
Zhukovsky, K. & Kalitenko, A. (2019*b*). *J. Synchrotron Rad.* **26**, 605–606.
Zhukovsky, K. & Kalitenko, A. M. (2019*c*). *Radiophys. Quantum Electron.* **62**, 52–64.
Zhukovsky, K. & Kalitenko, A. M. (2019*d*). *Russ. Phys. J.* **62**, 354–362.
Zhukovsky, K. & Potapov, I. (2017). *Laser Part. Beams* **35**, 326.